# Numerical Simulation of $CO_2$ Storage Potential with Enhanced Sedimentary Basin Characterization: A Case Study in Kazakhstan

**Bolatbek Khussain**
D.V. Sokolsky Institute of Fuel, Catalysis and Electrochemistry, Kazakhstan
b.khusain@ifce.kz

**Adel Sarsenova**
Kazakh Institute of Oil and Gas JSC, Kazakhstan
a.sarsenova@king.kz (corresponding author)

**Abzal Kenessary**
Kazakh Institute of Oil and Gas JSC, Kazakhstan
a.kenessary@king.kz

**Ranida Tyulebayeva**
Kazakh Institute of Oil and Gas JSC, Kazakhstan
r.tyulebayeva@king.kz

**Daniyar Abishev**
Kazakh Institute of Oil and Gas JSC, Kazakhstan
d.abishev@king.kz

**Tumen Darzhokov**
Kazakh Institute of Oil and Gas JSC, Kazakhstan
t.darzhokov@king.kz

**Saida Samigatova**
Kazakh Institute of Oil and Gas JSC, Kazakhstan
s.samigatova@king.kz

**Alexandr Brodskiy**
D.V. Sokolsky Institute of Fuel, Catalysis and Electrochemistry, Kazakhstan
albrod@list.ru

**Alexandr Sass**
D.V. Sokolsky Institute of Fuel, Catalysis and Electrochemistry, Kazakhstan
aleksandr-sass@mail.ru

**Viktor Martynov**
Kazakh Institute of Oil and Gas JSC, Kazakhstan
v.martynov@king.kz

*Received: 13 July 2025 | Revised: 10 August 2025 | Accepted: 22 August 2025*

 *DOI: https://doi.org/10.48084/etasr.13316*

## ABSTRACT

**Carbon Capture, Utilization, and Storage (CCUS) is globally recognized as a key strategy to mitigate the greenhouse gas emissions and address the climate change. Geological storage in oil and gas fields and saline aquifers offers a promising long-term solution, with growing research focusing on modeling, monitoring, and optimizing the storage performance. This study contributes to Kazakhstan's national CCUS initiative by presenting the methodology and outcomes of constructing a conceptual geological and hydrodynamic model of the Zaisan sedimentary basin located in East Kazakhstan. By integrating structural, lithological, and petrophysical data from 23 wells, a high-resolution 3D geological framework was developed. This model successfully identified a structurally isolated zone within the Sarybulak field that exhibits highly favorable characteristics for the CO2 storage, including minimal faulting, adequate reservoir thickness, high porosity, and high-water saturation. These features collectively highlight that the Sarybulak field is a highly promising candidate for Carbon Capture and Storage (CCS) deployment and reinforce the potential of the Zaisan basin as a strategic site for future large-scale carbon storage operations in Kazakhstan.**


***Keywords-$CO_2$; CCS; structural analysis; petrophysical analysis; $CO_2$ injection; lithological heterogeneity***

## I. INTRODUCTION

CCUS is a key strategy deployed to reduce the $CO_2$ emissions and mitigate the climate change. Among various approaches, the geological storage of $CO_2$ in saline aquifers, depleted oil fields, and unconventional reservoirs offers a promising long-term solution. Numerical simulations, geophysical monitoring, and machine learning techniques have been applied to evaluate the safety, efficiency, and feasibility of the $CO_2$ storage in different geological settings. These works explore the effects of reservoir heterogeneity, permeability, fault structures, and injection strategies on the $CO_2$ migration, trapping mechanisms, and storage performance. Despite progress, challenges remain in predicting the long-term behavior and ensuring the storage security. Continued research is essential to improve the modeling accuracy and support the large-scale deployment of CCUS technologies. Most countries are researching effective ways to store carbon dioxide in oil and gas reservoirs and to have reduced the gas emissions by 2060 to maintain the ecological stability.

### *A. $CO_2$ Storage*

Advances in geomechanical modeling and numerical simulation have enabled more accurate assessments of the geological formations for the carbon dioxide ($CO_2$) storage. A Stanford University study developed a detailed geomechanical model of the West Delta field in the Gulf of Mexico using PETREL, incorporating fluid flow and geomechanical equations to construct a three-dimensional representation [1]. The results demonstrated that the field holds potential for $CO_2$ storage, although injection was found to induce fault activity and alter reservoir properties, such as porosity and pressure, ultimately leading to the plastic deformation of the sandstone and migration toward the lowest porosity endcap. The need for further research with improved calculation accuracy was emphasized. Four of the six basins were studied and were deemed capable of storing approximately 539 Gt of $CO_2$ safely and effectively, with the added potential of increasing the oil recovery rates to 45%–60% through $CO_2$-Enhanced Oil Recovery ($CO_2$-EOR). Authors in [2] conducted field-scale numerical simulations of the Choszczno-Suliszewo brine aquifer in Poland, using seismic and well log data. Their work highlighted the importance of anisotropic permeability and facies-controlled flow in storage performance, concluding that the Lower Jurassic sandstone layers in the structure offer favorable conditions for the underground $CO_2$ storage. Authors in [3] employed the $CO_2$-SCREEN tool to assess the storage capacity of 17 sedimentary basins in Saudi Arabia, producing results aligned with the CSLF estimates. The Eastern Arabian Basin (EAB) and the Interior Homocline Central Arch (IHCA) were identified as having a high storage potential, while basins in the western and central regions showed considerably lower capacities due to less favorable geological characteristics. These studies collectively emphasize the critical role of advanced modeling, validated methodologies, and site-specific data in evaluating the feasibility and reliability of $CO_2$ sequestration in diverse geological environments.

### *B. Leakage and Risks*

Advanced monitoring and simulation methods have been explored to improve the safety and efficiency of CCUS operations. Authors in [4] focused on the application of the Time Domain Electromagnetic Method (TEM) for real-time monitoring of the $CO_2$ distribution and potential leakage pathways in subsurface formations. This method detects leakage by comparing the electrical resistivity of the rock layers, as $CO_2$ displaces the pore water and alters the electrical conductivity. The numerical simulations showed that anthropogenic factors could drive the upward migration of $CO_2$, which fills the pore space and causes detectable electrical changes. Additionally, TEM was proven to be effective in evaluating the geological characteristics of the reservoir, and one such experiment conducted in China was concluded successfully.

In [5], numerical simulations were developed to evaluate the behavior of $CO_2$ after 10 and 20 years of injection shutdown. Using $CO_2$-Enhanced Water Recovery ($CO_2$-EWR) and $CO_2$-EOR methods, the study assessed the recovery process and $CO_2$ migration over two decades. Natural monitoring tools with wide spatial coverage were utilized to detect possible leakages. Two leakage points were identified in drilling zones where faults acted as conduits for the $CO_2$ migration. Further investigation employed 4D modeling of the $CO_2$ injection into a saline aquifer, revealing pressure variations across a nine-layer trap and caprock structure during the injection phase [6]. The simulations indicated that the pressure buildup varied by layer, and that 20 years after

injection the dominant $CO_2$ storage mechanism had changed. After an additional 100 years, the volume of trapped $CO_2$ was found to have decreased, and discrepancies were observed between the simulation results and 4D seismic data. In a separate study, induced seismicity due to $CO_2$ injection was modeled using the Imperial College Geomechanics Toolkit (ICGT), a 3D finite-element simulator [7]. The simulation assessed the fault slip behavior within a multilayered geological setting characterized by permeabilities ranging from $10^{-14}$ to $10^{-19}$ $m^2$, over extended periods of fluid injection. By replicating a prior 2D model in three dimensions while adjusting the material properties and refining the mesh, the study confirmed that fault slip predictions were within a few cm of the observed values, contributing to an improved understanding of the seismic risks. Collectively, these studies underscore the importance of integrated geophysical monitoring, long-term simulation, and seismic risk assessment in ensuring the secure and sustainable implementation of CCUS technologies.

### *C. Reservoir Features*

Numerical and computational techniques have been employed to evaluate the feasibility and performance of $CO_2$ storage in various geological contexts. Authors in [8] assessed the $CO_2$ geological storage in the Yellow River Delta using numerical simulators, such as TOUGH2/ECO2N, incorporating environmental and spatial constraints, such as ecologically sensitive zones, drinking water sources, and protected areas. The simulation results revealed that $CO_2$ migration during injection followed a funnel-shaped distribution, with the lateral diffusion influencing all reservoir layers. The GIS-based proximity analysis and saline aquifer storage principles confirmed that the emission sources and sequestration targets could be fully covered within a 100 km radius.

The potential of the Amal Oil Field for $CO_2$ storage was explored in [9], where stratigraphic and structural analysis identified a horst block fault-bound trap as ideal for containment. The reservoir was found to possess favorable properties, including high effective porosity (PHIE), low shale volume, low water saturation, and sufficient permeability. Authors in [10] evaluated the $CO_2$ storage potential at multiple scales, basin, depression, play, and trap, noting that the theoretical capacity depends on the trapping mechanisms, while the engineering capacity is influenced by the injectivity, storage pressure, well count, and injection duration. Python libraries, such as Pandas and Openpyxl, enabled the efficient processing of large datasets, although the method relies heavily on high-quality input data. Supercritical $CO_2$ (SC-$CO_2$) fracturing was modeled in [11], with simulations capturing the heat transfer, flow, fracture propagation, and proppant transport. SC-$CO_2$ was shown to create more complex fracture networks with lower initiation pressures than the conventional hydraulic fracturing, while thicker SC-$CO_2$ and lightweight proppants improved the fracture width and proppant deployment. Authors in [12] modeled $CO_2$-foam injection using a hybrid thermodynamic framework combining the Peng–Robinson equation of state and an aqueous activity model. The results indicated enhanced gas trapping, reduced upward breakthrough, and increased sweep efficiency, especially with capillary transition zones. A hybrid modeling approach was presented in [13], which combined CMG-GEM simulations with Artificial Neural Networks (ANN), achieving 98% accuracy in predicting the $CO_2$ sequestration behavior while significantly reducing the computational time. Finally, authors in [14] examined the effect of the grid size on the $CO_2$ dissolution modeling, showing that coarse grids may overestimate the dissolution rates, emphasizing the need for appropriate grid selection and analytical model validation.

### *D. EOR and EGR*

Several studies have explored innovative numerical modeling approaches to improve the understanding and optimization of $CO_2$ injection processes for enhanced EOR and long-term sequestration. Authors in [15] employed Embedded Discrete Fracture Modeling (EDFM) to simulate the $CO_2$ injection in a layer-cake geological structure. They successfully completed a 20-year simulation within 1 h, demonstrating significantly higher computational efficiency compared to the conventional models. The study varied the matrix permeability from 0.0005 mD to 0.1 mD, resulting in substantial increases in cumulative oil production—120%, 279.6%, and 328.5%, respectively—highlighting the impact of permeability enhancement on the recovery performance.

Authors in [16] examined the $CO_2$ injection in Residual Oil Zones (ROZs) using geostatistical modeling and three-phase flow simulations. The study focused on geological heterogeneity, including permeability anisotropy, global heterogeneity, and autocorrelation, and their influence on the $CO_2$ movement and oil recovery. It was found that the increased heterogeneity and autocorrelation negatively affected both the recovery and sequestration by promoting the $CO_2$ channeling, while vertical permeability improved the sweep efficiency through gravity override. The $CO_2$ utilization ratio declined with greater heterogeneity but improved with increased permeability, suggesting targeted strategies for optimizing EOR and storage in ROZs. Authors in [17] analyzed the feasibility of SC-$CO_2$ injection in Longmaxi shale formations for combined enhanced gas recovery and $CO_2$ storage. Isothermal adsorption experiments, interpreted using the Ono-Kondo model, were used to describe the $CH_4$/$CO_2$ interactions, while a hybrid Discrete Fracture Network (DFN) and Multiple Interacting Continua (MINC) model simulated the complex fracture–matrix interactions. Realistic field conditions were modeled using a multiscale compositional approach solved by the Control Volume Finite Element (CVFE) method. The results demonstrated that SC-$CO_2$ Huff-n-Puff injection cycles significantly improved both the gas recovery and carbon sequestration efficiency. Furthermore, orthogonal experimental design was used to optimize the injection parameters, balancing the gas production and $CO_2$ retention. These studies collectively emphasize the critical role of geological heterogeneity, fracture complexity, and numerical efficiency in predicting and optimizing the $CO_2$ injection strategies for dual-purpose recovery and storage operations.

Authors in [18] explored optimization strategies for $CO_2$ Huff-n-Puff injection in shale reservoirs, demonstrating the role of porosity, permeability, and residual saturation in enhancing the gas recovery while ensuring containment [18]. They used

compositional simulation and emphasized the significance of integrating petrophysical analysis with reservoir modeling. Authors in [19] analyzed six other reservoirs of Kazakhstan by using the Carbon Sequestration Leadership Forum (CSLF) and U.S. Department of Energy (USDOE) methodologies, revealing that the $CO_2$ injection affects mineralogy through the dissolution and precipitation processes, as well as the porosity and trapping efficiency. Another study in Kazakhstan applied Python-based algorithms to assess CCUS in oil fields, highlighting the usefulness of the Dykstra-Parsons coefficient in evaluating the reservoir heterogeneity and improving the prediction accuracy [11].

Despite these global advances, limited efforts have been made to construct basin-scale geological models in Kazakhstan using modern digital tools. Most existing models are local and fail to incorporate lateral facies variability, which is crucial for defining the effective storage volumes. The present study addresses this gap by proposing a basin-wide conceptual model rooted in high-resolution petrophysical and structural inputs from the Sarybulak field.

## II. MATERIALS AND METHODS

As part of the study on the $CO_2$ storage potential at the Sarybulak field, a petrophysical investigation was carried out to characterize the lithological composition and reservoir rock petrophysical properties in detail. The primary objective was to develop a comprehensive petrophysical model that would provide a robust foundation for the numerical modeling of the $CO_2$ storage potential. The complexity of the petrophysical interpretation is driven by the high heterogeneity, intricate internal structure, and variable mineralogical composition of the reservoir. The productive intervals of the North-Zaisan Formation (C-Z-II) and the Triassic Tologoy Formation (T-I), which form a massive, stratified accumulation, represent the main prospective targets. The numerical modeling of the $CO_2$ storage potential was based on a detailed interpretation of well log data, core analysis, and cluster analysis conducted for wells C-101, C-111, and C-9.

### *A. Source Data and Research Methods*

The digitization of well log diagrams was performed for two areas of the Sarybulak field: the Central and Eastern sectors. The total number of wells with available logging data amounted to 25. The data were provided in the form of JPG image files. The objective of this stage was to convert analog data into a digital format for further petrophysical interpretation. The total footage of digitized log curves was 5,725 m. The following types of geophysical well logging were conducted in the analyzed wells: Gamma Ray (*GR*); Spontaneous Potential (*SP*); Neutron Porosity (*W*); Caliper Logging (*CALI*); Lateral log (*LL3*) and Multi-array Lateral Logs (*LLS, LLM, LLD*); Induction Log (*ILR*); Acoustic Log (*DT*); Density Log (*RHOB*); and Photoelectric Factor Log (*PEF*). Table I represents input data for the cluster analysis with intervals recorded from 3 wells and the geophysical surveys that were used.

The quality of well logging data was adversely affected by the large wellbore diameters (241 mm, 269.9 mm, 295.3 mm, and 393.7 mm) and by pronounced borehole washouts observed across many intervals of the productive sequence. For accurate calibration of the log data and more reliable interpretation of the geological structure, it is essential to account for the lithological characteristics of the section as identified from the core analysis.

TABLE I. DIGITIZED GEOPHYSICAL WELL LOG CURVES

| **Digitized geophysical well log curves** | | | |
|---|---|---|---|
| **Well No.** | **Geophysical well logging methods** | **Interval of recorded logs (m)** | |
| | | **Top** | **Base** |
| C-9 | *GR, W, LL3, ILR, RHOB, DT* | 1312 | 1650 |
| C-101 | *GR, W, SP, CALI, LLS, ILR, RHOB, DT, PEF* | 1190 | 1380 |
| C-111 | *GR, W, SP, CALI, LLS, LLM, LLD, RHOB, DT, PEF* | 1240 | 1460 |

The Akzhal Formation (T3ak) is characterized by the predominance of conglomerates (51%) composed of boulder-, coarse-, and fine-pebble material, with occasional interbeds of gravelstones and sandstones. A relatively uniform mineral composition is observed throughout the section in both the clastic and cementing components of the rocks. Sandstone interbeds are locally present in the lower part of the formation.

The section of the Tologoy formation (T3–J1tl) is composed mainly of sandstones of variable grain sizes (39%), siltstones, argillites (12%), sands (19%), and interbeds of carbonaceous shales and brown coals. This formation is characterized by the predominance of fine-grained clastic rocks (siltstones, argillites) over coarse-grained facies (sandstones, gravelstones), particularly in the lower part of the section [20].

The pie chart in Figure 1 illustrates the average lithological composition of the productive deposits of the Akzhal, Tologoy, and North-Zaisan formations at the field, based on macroscopic core descriptions. The dominant lithotype in the Akzhal Formation is conglomerate (51%), followed by sand (15%) and argillite (26%). In the Tologoy Formation, sandstones dominate (39%), with sand (19%), clay (12%), and gravelstone (9%) also being present. The North-Zaisan Formation is characterized by sand (13%), siltstone (11%), and sandstone (9%).

To define the criteria for classifying rocks as reservoir-quality, capillarimetry methods were employed, particularly centrifugation, to assess the pore space and fluid saturation [21, 22]. To determine the threshold values for *PHIE*—defined as the fraction of pore volume not occupied by irreducible water—the following relationship was used [23]:

$$\varphi_{eff} = \varphi_t \cdot (1 - S_{wi}) \quad (1)$$

where $\varphi_t$ is the total (open) porosity of the sample, and $S_{wi}$ is the irreducible water saturation.

Irreducible water saturation was determined experimentally using the semi-permeable membrane method on representative core samples taken from gas-saturated intervals in Horizons A (well C-29, central dome) and T-II (well C-101, eastern dome). The resulting data were used to construct plots showing the relationship between the *PHIE*, total porosity, and permeability.

The analysis of these plots revealed that at near-zero *PHIE*, the threshold values of the total porosity are 0.14 for the T3–J1T interval and 0.16 for the T2–3AKG interval, respectively, as seen in Figure 2(a). The threshold permeability, established from a combined graph for both intervals, was found to be 0.5 mD, as depicted in Figure 2(b).

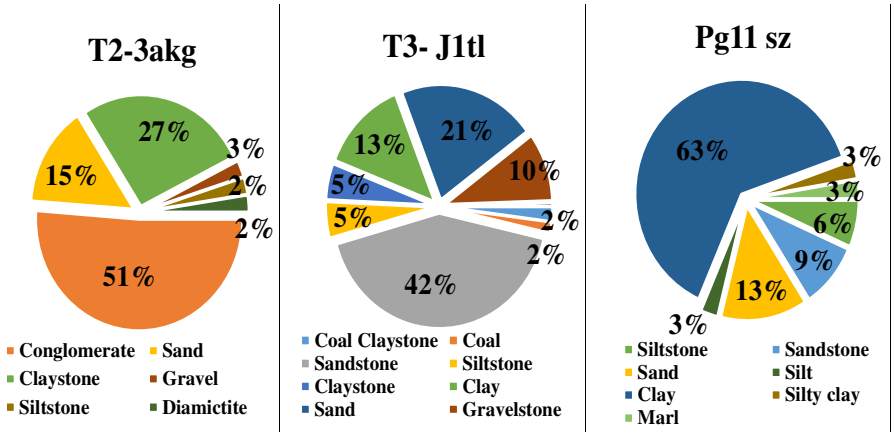


Fig. 1. Lithotype distribution based on core macroscopic description.

(a)

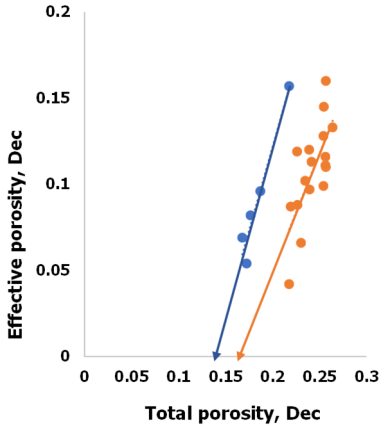


(b)

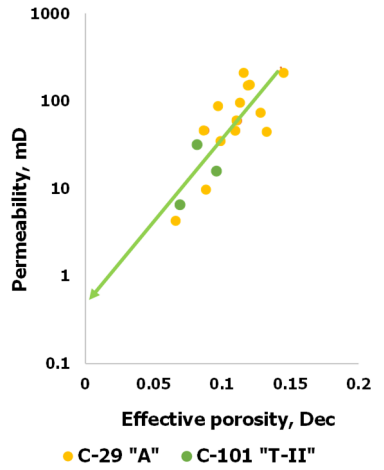


Fig. 2. Comparison of *PHIE* versus: (a) total porosity, (b) permeability.

## B. Well Log Interpretation

The interpretation was carried out using the specialized software Interactive Petrophysics. Reservoir identification was performed based on typical features of the terrigenous rocks, using an integrated approach that combined geophysical well log data, core analysis results, drill cutting descriptions, and formation testing data. The selection relied on qualitative indicators characteristic of terrigenous-type reservoirs, including reduced *GR* readings, increased *ΔT* values on sonic logs (*DT*), lowered density readings on density logs (*RHOB*), presence of radial resistivity gradients identified using multi-depth resistivity tools (*LL3, LLS, LLM, LLD, ILR*), and indications of clay-rich mudcake from caliper logs. When determining the effective thicknesses, dense, clay-rich, and carbonaceous interbeds were excluded from the total thickness.

The calculation of the Volume Clay Content (*VCL*) from *GR* logs was performed using the Larionov formula [24]:

$$VCL = 0.33 \cdot (2(2 + \Delta GR) - 1) \quad (2)$$

where $\Delta GR$ is the normalized gamma ray index, calculated using (fractional units):

$$\Delta GR = \frac{(GR - GR_{min})}{GR_{max} - GR_{min}} \quad (3)$$

The total (open) porosity from neutron log *W* was calculated by [23]:

$$\varphi_{neu} = W - VCL \times W_{clay} \quad (4)$$

where $W_{clay}$ is the hydrogen index of the clay content.

The total porosity from the density log (*RHOB*), corrected for the clay content, was calculated using [23]:

$$\varphi_{den} = \frac{(RHOB_m - RHOB)}{(RHOB_m - RHOB_f)} - K_{cl} \cdot \frac{(RHOB_m - RHOB_{cl})}{(RHOB_m - RHOB_f)} \quad (5)$$

where $RHOB_m$ is the matrix (mineral) density (2.68 g/cm$^3$), *RHOB* is the bulk density from the density log (gamma-gamma logging), $RHOB_f$ is the fluid density (1.0 g/cm$^3$), $K_{cl}$ is the clay density, and $RHOB_{cl}$ is the volumetric clay content ($V_{clay}$).

The porosity profiles were evaluated based on integrated analysis of neutron (*W*) and density (*RHOB*) logs. Figure 3 displays the clay volume and *PHIE* distribution for wells 101,

111, and C-9. The average value of the clay volume and *PHIE* accounted for 0.27 dec and 0.18 dec, respectively.

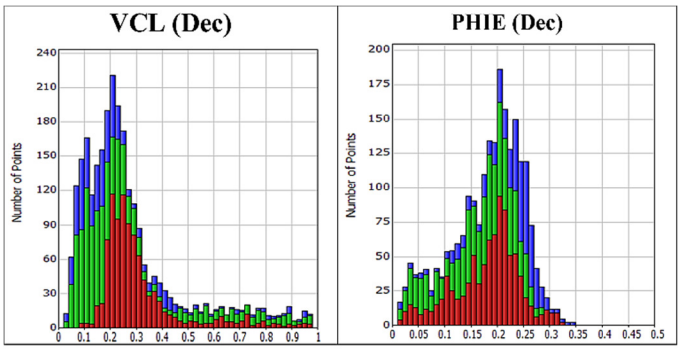


Fig. 3. Clay volume and *PHIE* distribution histograms for wells 101, 111, and C-9.

The permeability was calculated using an empirical formula [25]:

$$k = a \times \frac{\varphi^b}{S_w^c} \quad (6)$$

where $k$ is the permeability, $\varphi$ is the porosity, $S_w$ is the capillary-bound water saturation, and the empirical coefficients are: $a = 8581$, $b = 4.4$, and $c = 2$.

The validity of the petrophysical model was evaluated using a comparative analysis of the calculated log-derived curves and core laboratory measurements for the Tologoy Formation (T3–J1tl) in well C-101, as seen in Figures 4–6. The comparison demonstrates a high degree of correlation between the interpreted petrophysical parameters and core data, thereby confirming the robustness and consistency of the selected model and input parameters. The minor deviations observed in some intervals are likely attributable to the differences in the measurement scale (core versus log resolution) and the influence of the borehole irregularities, including washouts.

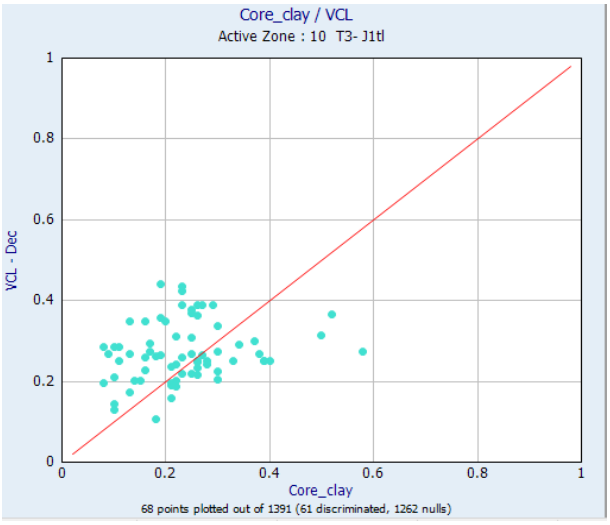


Fig. 4. Comparison of clay volume from core and log data.

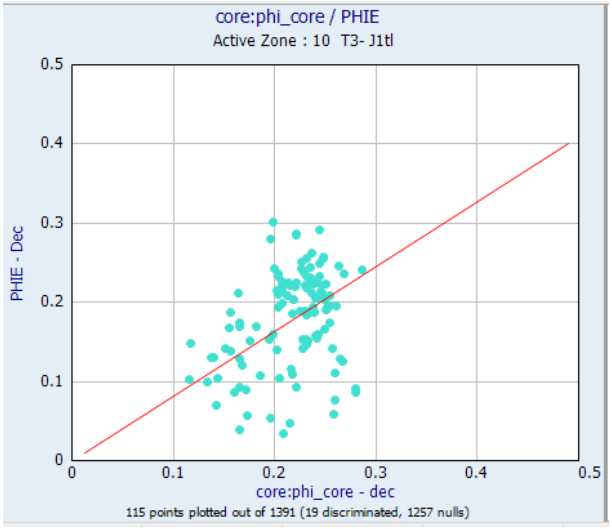


Fig. 5. Comparison of porosity from core and log data.

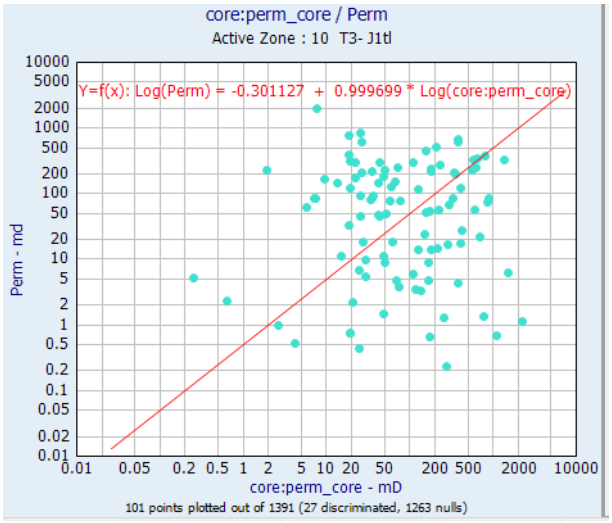


Fig. 6. Comparison of permeability from core and log data.

## C. Cluster Analysis

To automate the classification of the lithological types within the productive intervals and to evaluate their reservoir quality, the K-means clustering algorithm was applied. The input dataset included *GR, RHOB, DT, LL3, W, VCL*, and *PHIE* logs, which are known to be the most sensitive to the lithological variations [26]. The optimal number of clusters ($K$ = 7) was determined using the elbow method, supported by geological constraints. The selected number of clusters, corresponding to the inflection point on the elbow plot, provided a balanced trade-off between the lithological detail and statistical robustness [27]. The resulting clusters were cross-referenced with macroscopic core descriptions, enabling the identification of the following lithological types: clay, sandstone, sand, gravelstone, gravel, conglomerate, and coal.

Figures 7–9 illustrate the distribution of lithotypes in selected wells based on cluster analysis compared to the core description. The dominant lithological components vary across the studied wells: sandstone and conglomerate prevail in Wells

C-101 and C-9, while clay and sandstone dominate in Well C-111. These visualizations demonstrate the effectiveness of the clustering approach in capturing the heterogeneity of sedimentary facies and validate its consistency with core-based lithological interpretation.

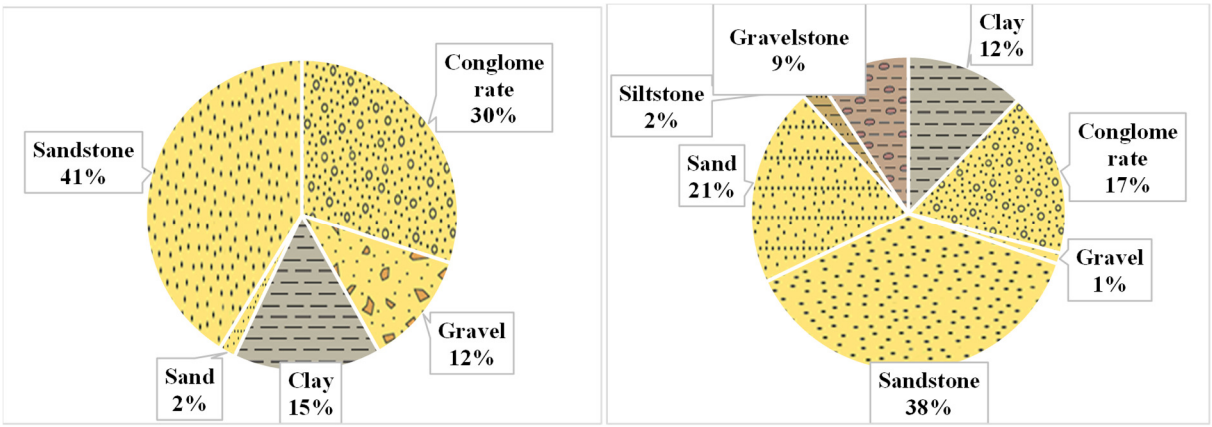


Fig. 7. Lithotype distribution comparison: cluster analysis versus core description for well C-101 (Tologoy Formation, T3–J1tl).

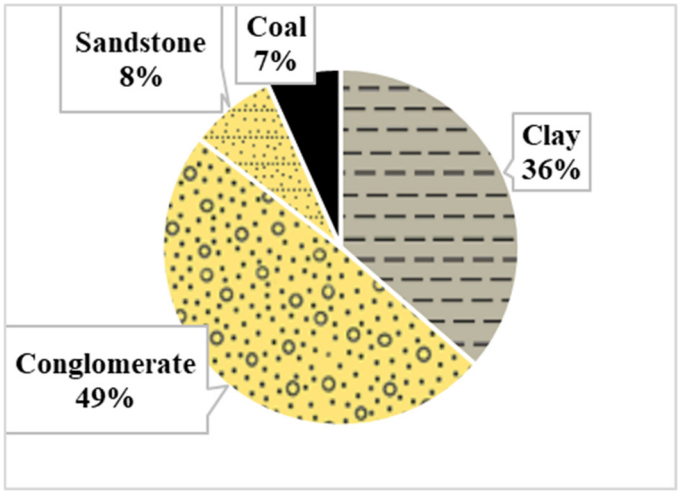


Fig. 8. Lithotype composition in well C-9 (Tologoy Formation, T3–J1tl).

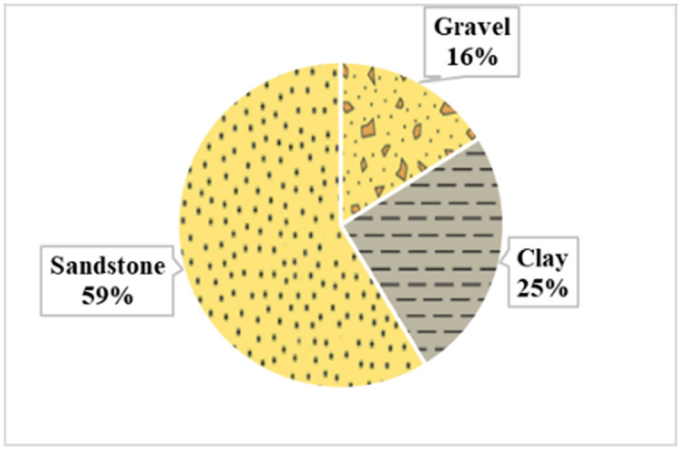


Fig. 9. Lithotype composition in well C-111 (Tologoy Formation, T3–J1tl).

### *D. Geological Modeling*

One of the key prerequisites for the safe and long-term geological storage of $CO_2$ is a comprehensive understanding of the regional stratigraphy and structural framework of potential reservoirs. The Zaisan sedimentary basin represents a promising geological setting for the CCS deployment in Kazakhstan. Its stratigraphic profile encompasses formations from the Devonian to Neogene periods. This includes a range of productive horizons:

- Paleocene units
- Jurassic intervals
- Triassic formations

These formations are characterized by alternating sandstones, siltstones, and clays deposited in fluvial-lacustrine and shallow marine environments. Thick clay-rich intervals above and below the reservoirs serve as effective regional seals. The presence of multiple reservoir–seal pairs enhances the potential for safe $CO_2$ injection and containment.

This study presents the construction of a conceptual geological model using Petrel software, based on log data from 23 wells of the Sarybulak field, regional structural maps, and petrophysical interpretation. The model serves as a foundation for selecting $CO_2$ injection sites and planning dynamic simulations within the Zaisan basin.

### *E. Geological Setting*

The Zaisan Basin is geologically associated with the eponymous depression, bounded by the southern spurs of the Altai Mountain system and the northern spurs of the Tarbagatai, Manrak, Saur, and Saikan ranges. The total area of the depression within Kazakhstan is about 30,000 $km^2$.

The basement of the depression, dating from the Devonian to Early Carboniferous, is exposed in the surrounding mountain structures and is characterized by a block-type structure. In the southern part of the Saur region, Middle to Upper Devonian

deposits form numerous small fields along the border between Kazakhstan and China. These include zones near the city of Zaisan and to the east and south of the village of Karaungir. The deposits consist of thick sequences of siliceous siltstones and shales with interbedded horizons of andesite-basalts and their tuffs. The total thickness of the deposits exceeds 2000 m.

The intermediate structural level consists of a Middle to Upper Carboniferous complex, dominated by sandstones, siltstones, carbonaceous siltstones, argillites, coals, and conglomerates. In the subsided parts of the basin, there are deposits of Permian to Middle Jurassic age. These are composed of siltstones, argillites, oil shales, and sandstones, with a thickness of about 350 m. Cretaceous deposits in the Zaisan Basin are represented by brownish-gray conglomerates, argillites, and siltstones. Above them, the sedimentary sequence is composed of Paleogene and Neogene deposits. The total thickness of the sedimentary cover reaches up to 6 km.

The reservoir intervals within the Sarybulak structure are distributed across a wide depth range, reflecting the complex stratigraphy of the Zaisan Basin. Paleocene gas-bearing horizons are typically encountered at depths of approximately 700-1000 m. Middle Jurassic reservoirs, likely corresponding to the J2kt horizon, occur within the interval of 1300-1500 m, where inflows of viscous oil and gas have been documented. Triassic deposits (T2-3akg), forming the basal part of the model, are found between 1550-1700 m, indicating deeper potential storage intervals. Permian sequences contain reservoir-quality sandstones and siltstones between 1850-2500 m, while the deepest stratigraphic units with hydrocarbon indications were identified between 2400-4100 m, confirming the presence of multi-level reservoir systems. This vertical heterogeneity provides favorable conditions for the $CO_2$ injection, offering both structural and stratigraphic containment.

### *F. 3D Geological Modeling*

The study focused on the Sarybulak field located in the northeastern sector of the Zaisan sedimentary basin. The input data comprised 23 LAS-format well logs obtained from the well logging results. These were processed using Interactive Petrophysics to derive the key reservoir properties: *PHIE*, Water Saturation (*Sw*), which were calculated using Archie's equation, and facies classification via self-organizing map clustering into five lithological categories.

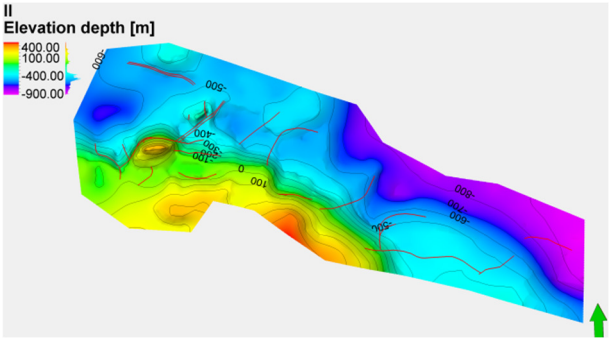


Fig. 10. Digitized seismic horizon II.

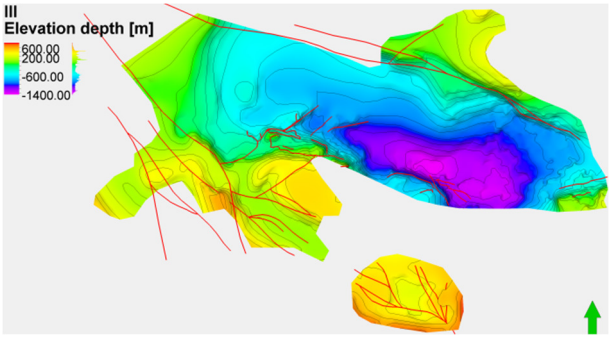


Fig. 11. Digitized seismic horizon III.

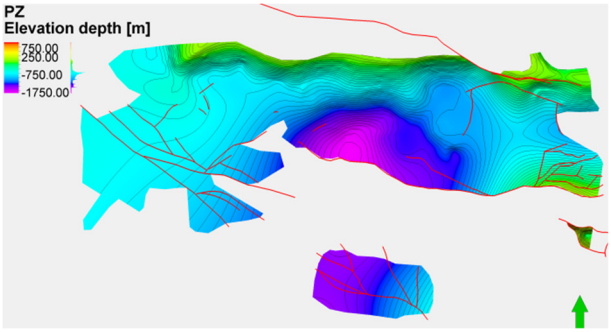


Fig. 12. Digitized seismic horizon IV.

The conceptual geological model of the Zaisan basin was developed using Petrel software, based on integrated geological, petrophysical, and geophysical data. Three main seismic horizons and faults were digitized from the reports: II – the top of the Turanginskaya suite $P_2tg$, III – the base of the Northern Zaisan suite, IV – the top of the Paleozoic $PZ_2$, as displayed in Figures 10–12. These horizons were used as trends when constructing structural surfaces. The modeling process relied on 23 wells with full logging suites, digitized and interpreted in the Interactive Petrophysics software. Three key stratigraphic surfaces were chosen as the structural framework of the model:

- $Pg11_{sz}$ – the Northern Zaisan formation of the Paleogene, representing the top of the modeled volume
- J2kt – Kustinskaya formation of the Middle Jurassic serving as the intermediate level
- T2-3akg – Triassic Akzhalskaya formation forming the base of the model

These three horizons were selected based on their regional mappability, petrophysical properties, and stratigraphic position. They represent major bounding surfaces that encapsulate the primary reservoir and seal complexes relevant to the $CO_2$ storage evaluation.

The conceptual model was constructed in a series of stages:

- Well correlation: The detailed correlation across 23 wells allowed the identification of the reservoir units and sealing intervals. Figure 13 shows the well correlation logs.

- Structure modeling: Using digitized structural contours and well tops, while surfaces for key stratigraphic horizons were built, as presented in Figure 14.

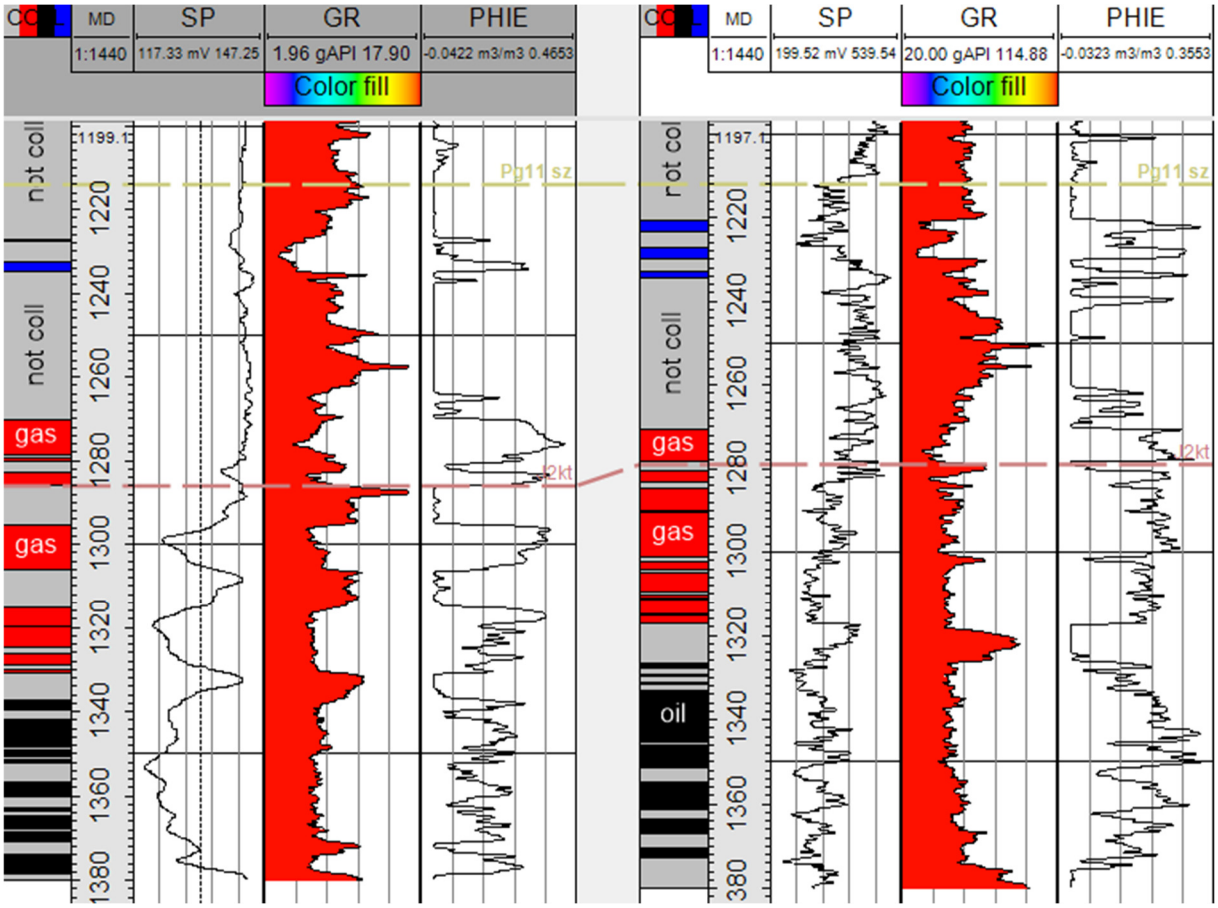


Fig. 13. Correlated well logs: (a) Hydrocarbon column, (b) SP, (c) GR, (d) PHIE.

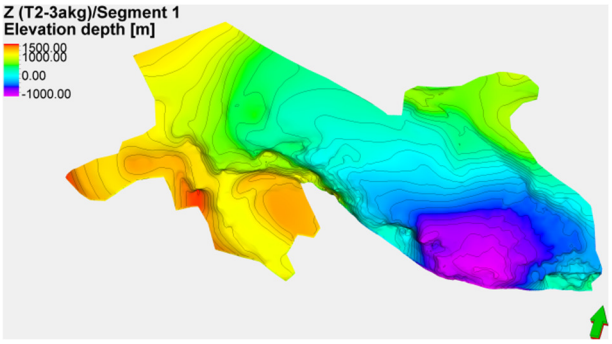


Fig. 14. Stratigraphic surfaces.

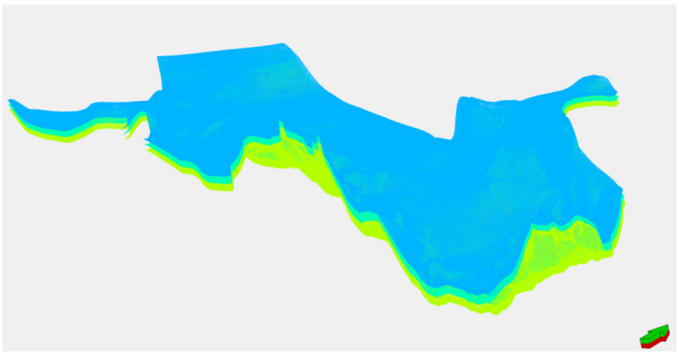

Fig. 15. 3D structural grid over the Zaisan basin.

- Structural grid generation, zone making, and layering: In modeling, the fundamental stage is the creation of a 3D grid, which is a framework of cells with a set of digital geological data. A correctly constructed three-dimensional grid is the basis for creating a correct geological model. Proportional layering and follow base were used for the upper and lower zones, respectively. The 3D structural grid over the Zaisan basin is depicted in Figure 15.

The total number of cells is 150 million. The cell thickness is 3 m for the upper zone ($Pg11_{sz}$) and 10 m for the lower zone (J2kt). More detailed grid parameters are shown in Table II.

The grid consists of two major zones, each constructed with different layering logic:

- $Pg11_{sz}$ – J2kt: subdivided using proportional layering into 20 layers, accounting for geometrical thinning/thickening trends based on structural surfaces.

- J2kt – T2-3akg: divided using constant vertical thickness (10 m) to ensure better control in deeper sections.

A total of 66 layers ensures sufficient vertical resolution for the facies distribution and property modeling. Volume correction was applied during the zone construction to maintain the stratigraphic balance. The grid respects all structural surfaces and accommodates minor dips and undulations typical of basin interiors.

TABLE II. 3D GRID PARAMETERS

| **3D grid parameters** | |
|---|---|
| Grid dimensions | 2150 × 1055 × 66 |
| Total number of cells | 149,704,500 |
| Number of geological horizons | 67 |
| Number of geological layers | 66 |
| Average call dimensions X (m) | 100 |
| Average call dimensions Y (m) | 100 |
| Average call dimensions Z (m) | 5.89 |

These discretization parameters were selected to optimize the accuracy while maintaining the computational efficiency for subsequent static-to-dynamic model transitions. The model supports petrophysical property propagation, facies simulation, and flow-based $CO_2$ injection studies across the selected geological domains. Scale up well logs: at this stage of constructing a three-dimensional geological model, work was carried out to transfer (average, upscaling) well data to 3D cells that intersected the well trajectory. The cells of the geological grid, opened by the well trajectory, were determined automatically based on the well trajectory data and the geometry of the 3D grids. For further description of the cubes, the lithology and porosity log curves were transferred to the cells.

### *G. Facies Modeling*

Facies modeling is a critical component of the geological modeling, especially in the context of $CO_2$ geological storage projects, where reservoir heterogeneity and caprock continuity play key roles in ensuring secure long-term containment. For the Sarybulak site, a lithofacies model was constructed to reflect the alluvial fan depositional environment, which dominates the central part of the Zaisan Basin. Facies classification and clustering were initially performed using petrophysical cluster analysis in Interactive Petrophysics software. Based on core descriptions and log-derived parameters, such as gamma-ray, density, neutron porosity, and resistivity, six principal lithologies were identified: clay, sandstone, sand, gravel, conglomerate, and coal. These lithotypes were interpreted as characteristic of an alluvial fan system, as presented in Figure 16, with proximal coarse-grained deposits (gravel and conglomerate) grading laterally into sand, sandstone, and distal mud-rich zones. Figure 17 illustrates the interpreted facies bodies generated from clustering, representing the expected sedimentary architecture. The coarse-grained units (in red) dominate the western and central parts of the fan, interpreted as high-energy braided channel deposits, while finer-grained sediments dominate the outer flanks. These geometries directly influence the porosity and permeability distribution, and thus the location and quality of potential injection targets.

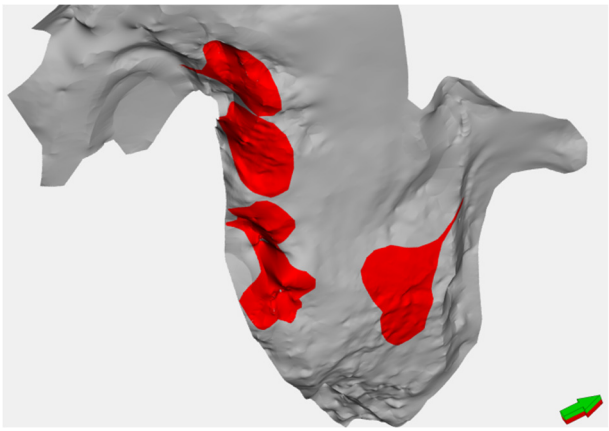

Fig. 16. Alluvial fan model.

To account for geological uncertainty and lateral variability, a stochastic facies simulation was performed in Petrel. The result is a detailed 3D facies cube that honors well data and reproduces realistic depositional patterns across the study area. Figure 17 displays the final facies model, where the lithologies are color-coded: purple for coal, grey for shale, yellow for sandstone, red for gravel and conglomerate, and orange for sand. This view demonstrates the heterogeneity of the Sarybulak subsurface. Coarse-grained facies, such as gravel and sandstone, are found in discontinuous, channel-like geometries. Their spatial arrangement reveals discrete zones of reservoir-quality rock, which are critical for the $CO_2$ storage. The facies model provides essential input for the subsequent porosity, permeability, and saturation modeling and serves as a geological basis for the dynamic flow simulation. The culmination of facies modeling is the creation of the lithology cube or Net-To-Gross (NTG) model, as shown in Figure 10. This cube serves as a Boolean filter in the geological model, defining where the reservoir rock (NTG = 1) exists and where non-reservoir materials (NTG = 0) are present. The NTG cube is indispensable for volumetric estimation and for initializing the dynamic $CO_2$ injection models (Figure 18).

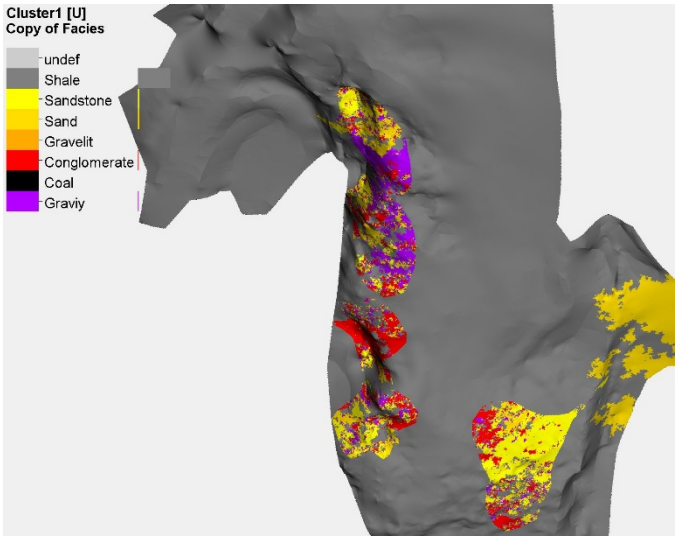


Fig. 17. Facies model.

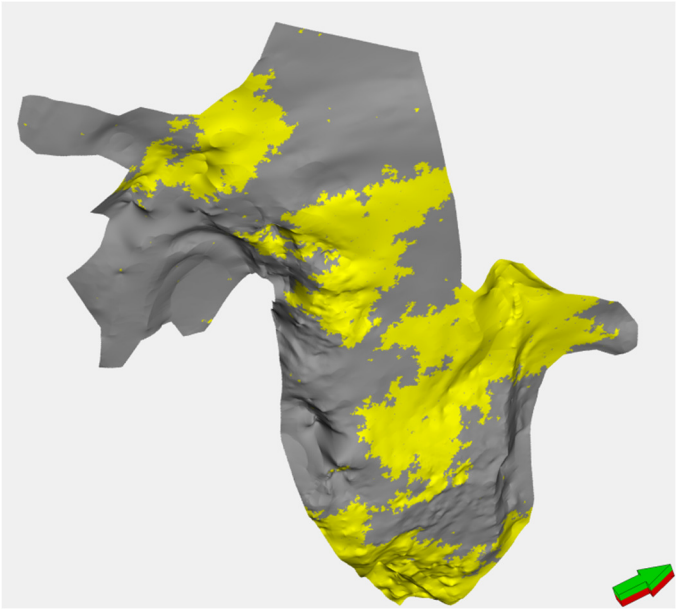

Fig. 18. The lithology cube.

The yellow regions indicate the presence of reservoir rocks, predominantly sandstones and gravels. These areas are spatially extensive in the central and southern domains, where the net thickness exceeds 15 m–20 m. In contrast, the gray regions represent non-reservoir facies, such as shale, coal, and clay, which act as internal baffles or seals, limiting the vertical migration. This binary classification enables the clear identification of injectivity windows and containment boundaries.

The facies modeling in this study fulfills multiple objectives:

- It delineates the spatial distribution of key reservoir facies, identifying zones with favorable injectivity characteristics.
- It establishes the heterogeneity structure required for accurate reservoir property upscaling and flow simulation.
- It supports risk assessment and site selection, ensuring that only zones with sufficient lateral continuity and vertical confinement are considered for injection.

In summary, the facies model forms the geological backbone of the $CO_2$ storage simulation workflow. It integrates petrophysical interpretation, depositional environment reconstruction, and geostatistical modeling, ultimately guiding the definition of secure and effective injection zones in the Zaisan basin.

### *H. Petrophysical Modeling*

A porosity model was developed using Sequential Gaussian Simulation (SGS) in Petrel, integrating interpreted *PHIE* values from 23 wells and the results of lithofacies clustering. High-porosity zones (up to 20%) are primarily located in the central and northwestern sectors of the Sarybulak field, aligning with coarse-grained fluvial channel deposits.

These values are in good agreement with the geological and petrophysical data presented in the regional report, where the Jurassic J2kt horizon is described as having porosity values between 0.12 and 0.18, with local enhancements in sandy bodies. The Triassic T2-3akg horizon exhibits lower porosity (0.08–0.12) but is laterally extensive and lithologically consistent, providing a secondary storage candidate.

The model reflects sedimentary heterogeneity, with reduced porosity in floodplain and overbank facies zones. These distinctions are critical for evaluating the $CO_2$ storage capacity and optimizing the injection placement. The absence of significant faulting and the presence of a gentle regional dip ensured the smooth property propagation across the structural grid, as seen in Figure 19.

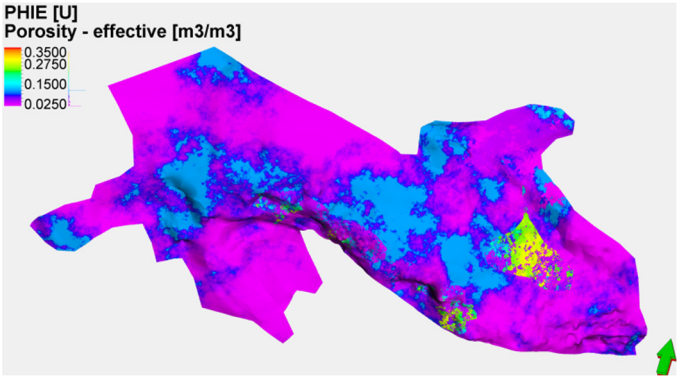


Fig. 19. Porosity model.

The constructed structural framework of the Zaisan basin allowed the simulation of regional depositional trends and the identification of a structurally stable site southeast of the basin, proposed as a potential $CO_2$ injection zone (Figure 20).

The image displays the spatial correlation between the favorable lithofacies (yellow – sandstone, red – gravel/conglomerate) and the boundaries of the proposed injection area, outlined in black. These zones are characterized by laterally continuous sand- and gravel-dominated intervals embedded within a fine-grained matrix, which serves as an effective seal.

This region was selected based on a combination of geological stability, distance from production wells, and petrophysical favorability. It lies outside of the faulted zones and exhibits low structural dip, reducing the risk of $CO_2$ migration along inclined strata. The presence of coarse-grained facies ensures sufficient injectivity, while overlying mudstones and clay-rich facies offer vertical containment.

The facies architecture within the selected domain is consistent with channelized alluvial fan systems, where stacked reservoir bodies provide high porosity and permeability intervals—ideal for $CO_2$ plume expansion. These attributes were confirmed by the facies cube and lithology (NTG) model, ensuring robust injectivity and storage potential.

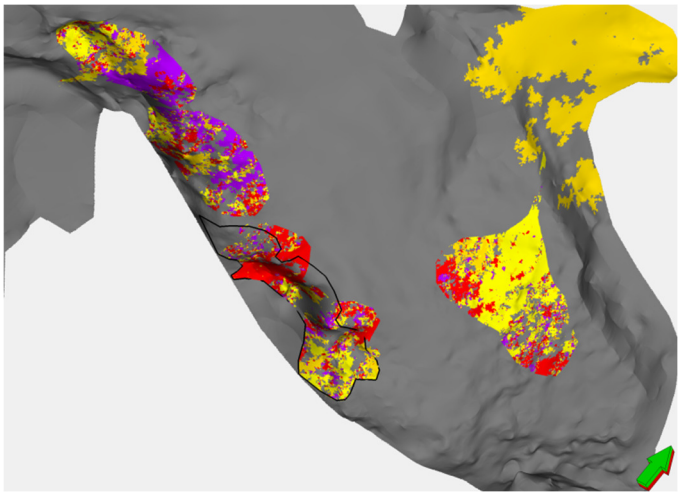

Fig. 20. Highlighted zone for detailed $CO_2$ injection analysis.

This proposed zone will serve as the target region for dynamic reservoir simulation, enabling the quantitative assessment of the $CO_2$ plume behavior, pressure distribution, and long-term containment integrity under various injection scenarios.

### *I. Numerical Simulation*

This part presents the construction and simulation of a $CO_2$ injection into the gas reservoir using the $CO_2$ SOL option in tNavigator software. A compositional simulation was applied, using basic input data for the fluid and rock properties.

A static geological model was imported into tNavigator, consisting of porosity distribution and structural geometry. No measured permeability model was available; instead, permeability was derived from porosity using the following exponential correlation:

$$K_{perm} = 0.033e^{36.844\emptyset} \quad (7)$$

where $\emptyset$ is the porosity (fraction), $K_{perm}$ is the permeability in md.

Due to the absence of laboratory-measured PVT data, default tNavigator fluid properties for pure $CO_2$ were used. The equation of state was set to Peng-Robinson. No additional gas components or salinity effects were included. The following key $CO_2$ parameters were used:

- Molecular weight: 44.01 kg/kmol
- Critical temperature: 304.19 K
- Critical pressure: 73.82 bar
- Acentric factor: 0.228

The simulation was conducted under the assumption that the field is a fully depleted gas reservoir. At the start of the model, the reservoir was considered completely saturated with formation water, representing post-production conditions where all original gas had been extracted. The datum depth of the model was set at 1063.84 m, and the corresponding initial reservoir pressure was 106.38 bar.

To assess the feasibility of $CO_2$ injection and storage, a subsection of the full reservoir model was extracted, specifically covering the eastern structural block, as depicted in Figure 21. This simulation domain contained 65909 active grid blocks.

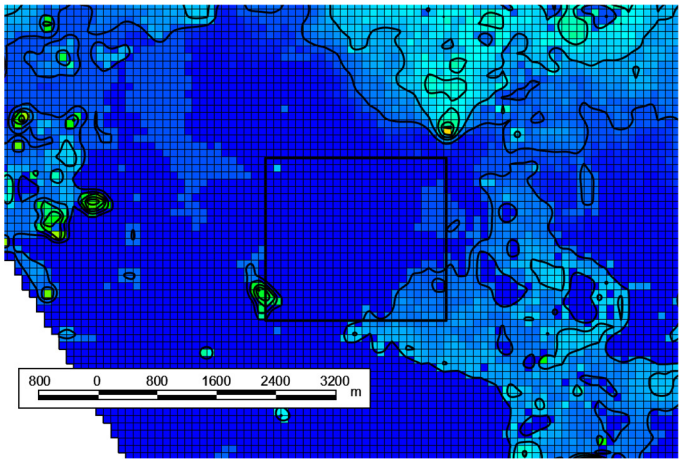


Fig. 21. Simulation domain cutout for eastern reservoir block.

A 9-point well pattern, as illustrated in Figure 22, was implemented in which all nine wells functioned as injection wells. The $CO_2$ injection was simulated at a constant total rate of 1,500,000 $sm^3$/day, equally distributed across the injection wells. The injection phase lasted for 1 year, followed by a 100-year post-injection monitoring period to analyze the long-term $CO_2$ migration, dissolution, and trapping mechanisms.

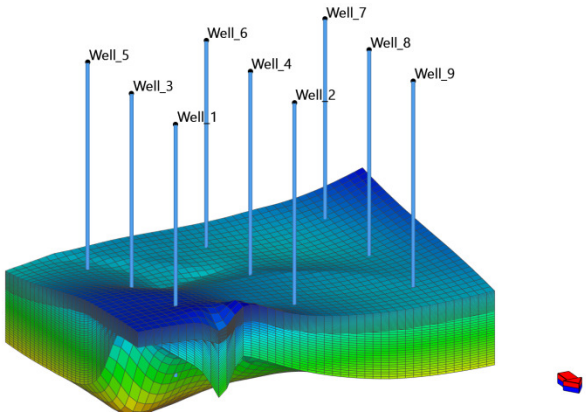


Fig. 22. 3D structural grid with 9-point $CO_2$ well pattern.

The model accounted for the following trapping mechanisms (Massarweh and Abushaikha, 2024):

- Structural trapping: accumulation beneath low-permeability, low-porosity zones
- Residual trapping: modeled using hysteresis between drainage and imbibition curves
- Solubility trapping: $CO_2$ dissolving into formation water as a function of pressure

## III. RESULTS

The $CO_2$ plume dynamics were assessed using vertical cross-sections of the simulation domain at three key moments: the beginning of injection, the end of the 1-year injection phase, and after 100 years of post-injection monitoring. The simulation tracked two main components: $CO_2$ dissolved in water and mobile $CO_2$ in the gas phase.

Figure 23 shows the vertical distribution of $CO_2$ at the start of injection. The gas remains near the well perforations with minimal movement. After 1 year, the $CO_2$ has migrated vertically and laterally, forming plumes that remain structurally confined, as portrayed in Figure 24. Figure 25 demonstrates that after 100 years of shut-in, the $CO_2$ remains trapped within the reservoir, with increased dissolution and reduced mobile gas volume.

A mass balance plot, exhibited in Figure 26, illustrates the temporal evolution of the $CO_2$ distribution. Mobile gas peaks early during injection and then declines as $CO_2$ dissolves into water. Solubility trapping becomes the dominant mechanism over time, confirming the long-term retention of injected gas.

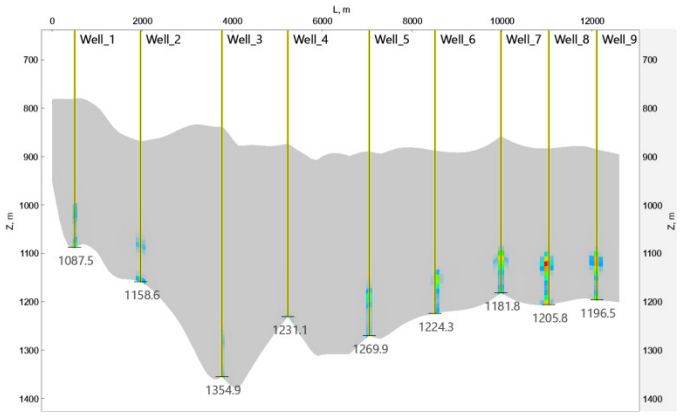


Fig. 23. Vertical cross-section showing $CO_2$ presence at the start of injection.

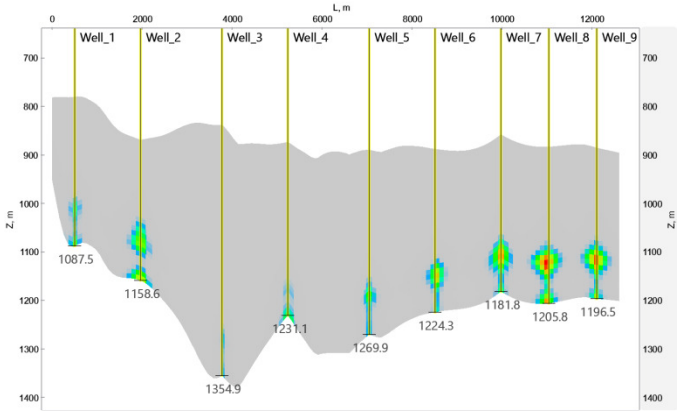


Fig. 24. Vertical cross-section showing $CO_2$ plume at the end of injection (1 year).

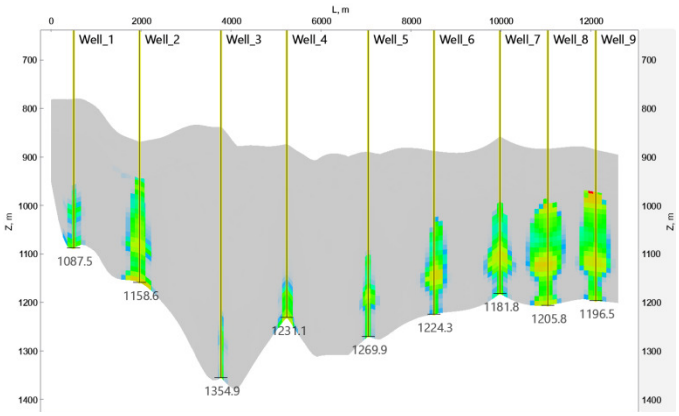


Fig. 25. Vertical cross-section showing $CO_2$ distribution after 100 years.

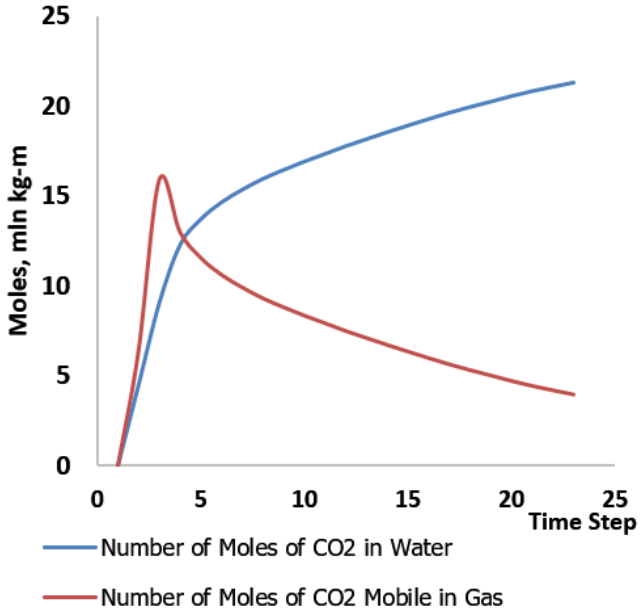


Fig. 26. Evolution of $CO_2$ moles in water and mobile gas phases over time.

A total of 600 million $sm^3$ of $CO_2$ were injected into the reservoir. By the end of the 100-year storage period, approximately 505.684 million $sm^3$ of the injected $CO_2$ (84.28%) had dissolved into the formation water, demonstrating the strong influence of the solubility trapping mechanisms. The remaining 94.32 million $sm^3$, or 15.72%, remained as free-phase gas, securely retained within the structural traps of the reservoir.

### A. *Limitations*

One of the observed limitations was the reduced performance of injection around Wells 3 and 4. As observed in Figure 28, the mesh structure in this area may have introduced local grid distortion, reducing the connectivity and injectivity in these zones. This limitation highlights the importance of the mesh quality and alignment in grid-based simulations. Thus, it should be addressed in future model refinements.

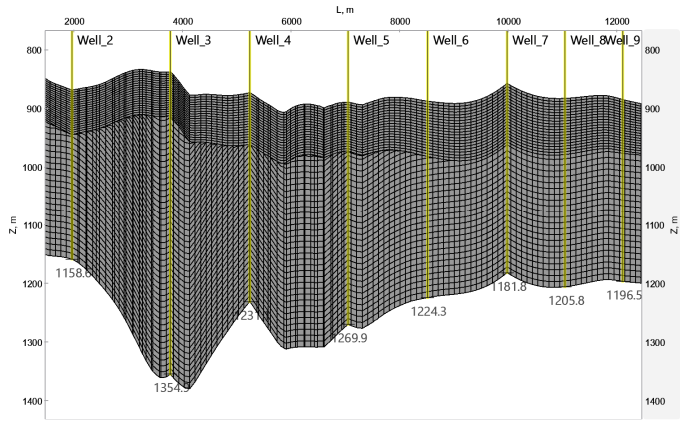


Fig. 27. Mesh resolution and structural complexity along well trajectories

## IV. CONCLUSION

The petrophysical analysis enabled the development of a detailed reservoir model that accounts for complex lithological composition and heterogeneity of the Akzhal and Tologoy formations. Key reservoir thresholds for porosity and permeability were established, while the model's validity was confirmed through consistent well log and core data comparisons. Furthermore, the application of K-means clustering facilitated the classification of principal lithotypes, enhancing the assessment of the reservoir quality.

Geologically, the integration of structural, lithological, and petrophysical data produced a coherent conceptual model that delineates reservoir units, sealing layers, and fault systems across the basin. The model identifies a structurally isolated area characterized by minimal faulting, sufficient reservoir thickness, and favorable porosity – features essential for the effective $CO_2$ injection and containment.

To further assess the basin's potential for Carbon Capture and Storage (CCS), numerical simulations were conducted using the $CO_2$ SOL module in tNavigator. A synthetic case assumed full depletion and water saturation of the reservoir at initial conditions. A porosity-based permeability model and default fluid properties were employed to simulate the $CO_2$ injection. The 9-point injection well layout allowed for a uniform $CO_2$ distribution, effectively representing key trapping mechanisms. This simulation approach proves suitable for early-phase CCS screening, particularly in reservoirs with limited available data, and confirms that the selected area within the Sarybulak field possesses the necessary properties to serve as a safe and efficient $CO_2$ storage site.

The study of the Sarybulak field and the broader Zaisan sedimentary basin has resulted in a conceptual framework to support future CCS initiatives. It closely aligns with global research trends in $CO_2$ geological storage. Similarly to international case studies that rely on integrated geological, petrophysical, and geomechanical modeling, the current research combines high-resolution lithological and structural data to construct a basin-scale conceptual model. The study reinforces the global consensus, according to which, robust site characterization is fundamental to ensuring the storage security. At the same time, it addresses the specific regional challenge of scaling from local to basin-level models, thereby supporting Kazakhstan's readiness for large-scale CCA deployment. The novelty of this study lies in its integration of high-resolution petrophysical analysis, basin-scale structural interpretation, and hydrodynamic simulation to identify an optimal $CO_2$ storage site–representing the first such application in the context of the Zaisan basin and setting a precedent for national-scale CCS resource mapping in Kazakhstan.

## ACKNOWLEDGMENT

The research was funded by the Committee of Science of the Ministry of Science and Higher Education of the Republic of Kazakhstan (Grant No. BR21882241).

## REFERENCES

[1] S. S. Hashemi and A. Kovscek, "Numerical Simulation of CO2 Storage in the Soft Sediments of Depleted Reservoirs in the Gulf of Mexico," in *SPE Western Regional Meeting*, Palo Alto, California, USA, Apr. 2024, Art. no. D031S014R005, https://doi.org/10.2118/218908-MS.

[2] J. Ye *et al.*, "Evaluation of Geological CO2 Storage Potential in Saudi Arabian Sedimentary Basins," *Earth-Science Reviews*, vol. 244, Sept. 2023, Art. no. 104539, https://doi.org/10.1016/j.earscirev.2023.104539.

[3] H. Yang *et al.*, "Numerical Simulation on CO2 Geology Storage Based on Transient Electromagnetic Theory," *Frontiers in Energy Research*, vol. 12, Dec. 2024, Art. no. 1494735, https://doi.org/10.3389/fenrg.2024.1494735.

[4] Y. Diao, X. Ma, C. Zhang, X. Jin, X. Li, and C. Zhang, "CO2 Geological Storage in Sedimentary Basins: An Update on the Potential and Suitability Evaluation and a Field Test," *Energy Geoscience*, vol. 6, no. 1, Mar. 2025, Art. no. 100369, https://doi.org/10.1016/j.engeos.2024.100369.

[5] T. Akai, T. Kuriyama, S. Kato, and H. Okabe, "Numerical Modelling of Long-term CO2 Storage Mechanisms in Saline Aquifers Using the Sleipner Benchmark Dataset," *International Journal of Greenhouse Gas Control*, vol. 110, Sept. 2021, Art. no. 103405, https://doi.org/10.1016/j.ijggc.2021.103405.

[6] J. E. J. Burtonshaw, A. Paluszny, and R. W. Zimmerman, "Numerical Modelling of Induced Seismicity Along a Fault During CO2 Injection into a Subsurface Reservoir," presented at the 15th ISRM Congress, Oct. 2023, Art. no. ISRM-15CONGRESS-2023-466.

[7] W. Sun, W. Liu, S. Ren, G. Lin, C. Wang, and X. Jiang, "CO2 Geological Storage Site Selection and Long-term Potential Assessment Framework Based on TOUGH2/ECO2N," *PLOS One*, vol. 20, no. 4, Apr. 2025, Art. no. e0321715, https://doi.org/10.1371/journal.pone.0321715.

[8] M. Amer, W. M. Mabrouk, A. M. Eid, and A. Metwally, "3D Seismic Modeling of the Amal Oil Field to Evaluate CO2 Storage Potential in Depleted Reservoirs, Southern Gulf of Suez," *Scientific Reports*, vol. 15, no. 1, May 2025, Art. no. 18334, https://doi.org/10.1038/s41598-025-03032-5.

[9] Y. Li, R. Wang, Q. Zhao, Z. Xue, and Y. Zhou, "A CO2 Storage Potential Evaluation Method for Saline Aquifers in a Petroliferous Basin," *Petroleum Exploration and Development*, vol. 50, no. 2, pp. 484–491, Apr. 2023, https://doi.org/10.1016/S1876-3804(23)60403-3.

[10] B. Khusain *et al.*, "A Python-based Evaluation of Kazakhstan's Fields for Carbon Capture, Utilization, and Storage Projects," *Engineering, Technology & Applied Science Research*, vol. 15, no. 2, pp. 20782–20789, Apr. 2025, https://doi.org/10.48084/etasr.9613.

[11] L. Wu *et al.*, "Numerical Simulations of Supercritical Carbon Dioxide Fracturing: A Review," *Journal of Rock Mechanics and Geotechnical Engineering*, vol. 15, no. 7, pp. 1895–1910, July 2023, https://doi.org/10.1016/j.jrmge.2022.08.008.

[12] X. Lyu, D. Voskov, and W. R. Rossen, "Numerical Investigations of Foam-assisted CO2 Storage in Saline Aquifers," *International Journal of Greenhouse Gas Control*, vol. 108, June 2021, Art. no. 103314, https://doi.org/10.1016/j.ijggc.2021.103314.

[13] M. Hamed and E. Shirif, "Sustainable CO2 Storage Assessment in Saline Aquifers Using a Hybrid ANN and Numerical Simulation Model Across Different Trapping Mechanisms," *Sustainability*, vol. 17, no. 7, Mar. 2025, Art. no. 2904, https://doi.org/10.3390/su17072904.

[14] M. Zeidouni, "Closed-form Analytical Approaches to Constrain Fraction of Injected CO2 Dissolving in Brine During CO2 Storage in Saline Aquifers," in *Proceedings of the 2025 Carbon Capture, Utilization, and Storage Conference*, Houston, Texas, United States, 2025, https://doi.org/10.15530/ccus-2025-4174810.

[15] Q. Yan, D. Shan, and K. Mansour, "Advanced Numerical Simulation of CO2 Storage in Depleted Unconventional Reservoirs with Enhanced Embedded Discrete Fracture Modelling (EDFM)," in *SPE Advances in Integrated Reservoir Modelling and Field Development Conference and Exhibition*, Abu Dhabi, UAE, June 2025, Art. no. D021S008R001, https://doi.org/10.2118/225318-MS.

[16] Y.-Y. Wang *et al.*, "Reservoir Heterogeneity Controls of CO2-EOR and Storage Potentials in Residual Oil Zones: Insights from Numerical Simulations," *Petroleum Science*, vol. 20, no. 5, pp. 2879–2891, Oct. 2023, https://doi.org/10.1016/j.petsci.2023.03.023.

[17] R. Zhang, J. Wu, Y. Zhao, X. He, and R. Wang, "Numerical Simulation of the Feasibility of Supercritical CO2 Storage and Enhanced Shale Gas Recovery Considering Complex Fracture Networks," *Journal of Petroleum Science and Engineering*, vol. 204, Sept. 2021, Art. no. 108671, https://doi.org/10.1016/j.petrol.2021.108671.

[18] B. Khusain, N. E. Zhumakhanova, A. Zh. Kenessary, D. N. Delikesheva, and T. D. Darzhokov, "Optimization of $CO_2$ Huff-n-puff Parameters for Enhanced Gas Recovery in Shale Reservoirs: A Compositional Simulation Study," *News of the National Academy of Sciences of the Republic of Kazakhstan*, vol. 3, no. 471, pp. 281–298, 2025.

[19] T. Urych, J. Chećko, M. Magdziarczyk, and A. Smoliński, "Numerical Simulations of Carbon Dioxide Storage in Selected Geological Structures in North-Western Poland," *Frontiers in Energy Research*, vol. 10, Feb. 2022, Art. no. 827794, https://doi.org/10.3389/fenrg.2022.827794.

[20] M. V. Li, "Report on Gas Reserves Estimation of the Sarybulak Field (East Kazakhstan Region of the Republic of Kazakhstan) as of 01.07.2017," LLP "Geoplazma", Aktobe, Kazakhstan, Technical Report, 2018.

[21] R. L. Slobod, A. Chambers, and W. L. Prehn, "Use of Centrifuge for Determining Connate Water, Residual Oil, and Capillary Pressure Curves of Small Core Samples," *Journal of Petroleum Technology*, vol. 3, no. 04, pp. 127–134, Apr. 1951, https://doi.org/10.2118/951127-G.

[22] E. C. Donaldson, R. F. Kendall, E. A. Pavelka, and M. E. Crocker, "Equipment and Procedures for Fluid Flow and Wettability Tests of Geological Materials," Department of Energy, Bartlesville, OK, USA. Bartlesville Energy Technology Center, United States, Technical Report DOE/BETC/IC-79/5, May 1980. [Online]. Available: https://www.osti.gov/biblio/5279717.

[23] D. Tiab and E. C. Donaldson, *Petrophysics: Theory and Practice of Measuring Reservoir Rock and Fluid Transport Properties*, Fourth edition. Amsterdam, Netherlands; BOS, USA: Elsevier/GPP, Gulf Professional Publishing is an imprint of Elsevier, 2016.

[24] V. V. Larionov, "Chapter 3," in *Borehole Radiometry*, Moscow, USSR: Nedra, 1969, pp. 65–70.

[25] A. Timur, "An Investigation of Permeability, Porosity, & Residual Water Saturation Relationships for Sandstone Reservoirs," *The Log Analyst*, vol. 9, no. 04, July 1968, Art. no. SPWLA-1968-vIXn4a2.

[26] J. H. Doveton, *Geologic Log Analysis Using Computer Methods*. OK, USA: American Association of Petroleum Geologists, 1994.

[27] R. Tibshirani, G. Walther, and T. Hastie, "Estimating the Number of Clusters in a Data Set Via the Gap Statistic," *Journal of the Royal Statistical Society Series B: Statistical Methodology*, vol. 63, no. 2, pp. 411–423, July 2001, https://doi.org/10.1111/1467-9868.00293.